Photonic Bose-Einstein Condensation in the Continuum Limit

Andris Erglis[*]

Physikalisches Institut, Albert-Ludwigs-Universität Freiburg, Hermann-Herder-Straße 3, 79104 Freiburg, Germany

Milan Radonjić

Institut für Theoretische Physik, Universität Hamburg, Notkestraße 9, 22607 Hamburg, Germany
and Institute of Physics Belgrade, University of Belgrade, Pregrevica 118, 11080 Belgrade, Serbia

Stefan Yoshi Buhmann

Institut für Physik, Universität Kassel, Heinrich-Plett-Straße 40, 34132 Kassel, Germany

We investigate the properties of the photon Bose-Einstein condensate in the limit of small mode spacing. Alongside the well-known threshold of the phase transition at large mode spacings, we find an emergence of a second threshold for sufficiently small mode spacings, defining the crossover to a fully condensed state. Furthermore, we present our findings for the mode occupations in the precondensate or supercooling region towards the continuum limit.

Introduction—The Bose-Einstein condensate (BEC) is a state characterized by a phase transition at a critical threshold above which the particles macroscopically occupy the lowest energy state. Typically, in experiments, the threshold for atomic BECs is the critical temperature [1,2]; for photons, it is the critical number of particles [3,4].

In photon BECs, the setup normally consists of slightly curved mirrors forming a cavity with dye molecules in between the mirrors. A fixed cavity length provides a quasi-two-dimensional (2D) setup with a transversal wave vector as the remaining degree of freedom. While a photon BEC can be achieved in such a confined setup, it is well known that in two dimensions, no condensation occurs in the thermodynamic limit, as the critical temperature (particle number) approaches zero (infinity) [5–8].

While many experimental and theoretical works study photon BECs within harmonic confinement mentioned above [3,9–17], recently, the photon BEC has also been demonstrated in a finite planar system with a 2D box potential [18]. Theoretically, an exhaustive description of the thermodynamical properties of a BEC has been given in [19], also demonstrating the formation of a BEC in a 2D box potential.

The difference between small and large system sizes has been previously considered in a 2D harmonic oscillator setup [20,21]. It was demonstrated via the photon-BEC rate equations that for smaller mode spacings, the ground state occupation has a sharper increase at the threshold, exhibiting a sign of thermodynamic limit. Another limit of highly anisotropic three-dimensional geometries has been studied

with massive bosons, where the phase transition into different condensation regimes was observed [22].

For a single mode, an analytical treatment of the photon BEC rate equations in adiabatic approximation has been given [23]. For small cavity decay rates, the photon number was found to be zero below a critical threshold while exhibiting a sharp transition into a condensate regime above the threshold with linear growth of the photon number.

The study of condensation in the continuum limit is also relevant to other systems with small mode spacing, e.g., chiral environments [23]. In such cases, the condensate properties will qualitatively differ compared to larger mode spacings. Without appropriate treatment of small spacings, one initially would not be able to see the formation of the condensate. Instead, the condensate will only emerge for experimental parameters far from the ones expected for large mode spacings.

In this Letter, we report our findings on the steady-state behavior of the photon BEC in a planar cavity at the crossover towards the continuum limit. Extending the analytical treatment of the photon BEC rate equations in Ref. [23] to two modes, we analytically find two critical thresholds marking the condensate formation. We corroborate our findings with numerical simulations for higher mode numbers and evaluate the critical number from thermodynamic principles for an infinite system, which we compare to the analytical solution. Finally, we demonstrate the behavior of photon occupation number in the precondensate or supercooling regime, which emerges in the limit of small mode spacing.

The model—We start by specifying the system geometry and the equations describing the photon BEC. Our model

---

[*]Contact author: andris.erglis@physik.uni-freiburg.de

223601-1

consists of a planar cavity where the control parameter is the transversal mode spacing $\Delta k^{\parallel}$ with the dispersion relation for the cavity mode frequency $\omega(j_x, j_y, \Delta k^{\parallel}) = c\epsilon^{-1/2}\sqrt{(j_z\pi/L_z)^2 + (j_x^2 + j_y^2)(\Delta k^{\parallel})^2}$, where c is the speed of light, ϵ is the relative permittivity of the cavity medium, j_z is the longitudinal mode number, L_z is the cavity length, j_x and j_y are transversal mode numbers in x and y directions, respectively, and $\Delta k^{\parallel}$ is defined as $\Delta k^{\parallel} = \Delta k_x = \Delta k_y = \pi/L$, where L is the length of the cavity mirrors in x and y directions. The ground mode is characterized by values $j_x = j_y = 1$.

As an inducer for effective photon-photon interaction, dye molecules are commonly used. Here, we rely on rhodamine 6G dye which fulfills the Kennard-Stepanov relation $\alpha_i = \epsilon_i e^{\beta\hbar(\omega_i - \omega_{ZPL})}$ where α_i and ϵ_i are the respective stimulated absorption and emission coefficients for mode i, ω_{ZPL} is the zero phonon line, and $\beta = 1/k_B T$ is the inverse temperature with $T = 300$ K. The rhodamine 6G spectrum [24], together with the position of the cavity modes, is shown in the Supplemental Material [25].

As the longitudinal mode spacing between the j_z and $j_z + 1$, $j_z - 1$ modes is comparable to the spectral width of the dye molecules, the cavity photons form a quasi-two-dimensional system with fixed longitudinal mode number j_z.

The rate equations describing the dynamics of the photon BEC can be obtained from the master equation using an open quantum systems description [26,27]. In adiabatic approximation with respect to the state of the dye molecules, the rate equations for the photon numbers n_i in mode i are given by

$$\dot{n}_i(\Gamma_{\uparrow}) = -\kappa n_i + M\frac{\epsilon_i\Gamma_{\uparrow}^{tot}(n_i + 1) - \alpha_i\Gamma_{\downarrow}^{tot}n_i}{\Gamma_{\uparrow}^{tot} + \Gamma_{\downarrow}^{tot}}. \quad (1)$$

Here, κ is the cavity decay rate, dependent on the reflectivity of cavity mirrors, M is the total number of molecules, $\Gamma_{\uparrow}^{tot} = \Gamma_{\uparrow} + \sum_{i=1}^{\mathscr{M}} g_i\alpha_i n_i$ is the total absorption rate with $\Gamma_{\uparrow}$ being the pumping rate of the molecules and g_i being the degeneracy of mode i. Similarly, $\Gamma_{\downarrow}^{tot} = \Gamma_{\downarrow} + \sum_{i=1}^{\mathscr{M}} g_i\epsilon_i(n_i + 1)$ is the total emission rate where $\Gamma_{\downarrow}$ is the spontaneous decay rate of the molecules. Photons emitted via spontaneous decay are lost from the system into noncavity modes. The $n_i + 1$ terms are responsible for stimulated and spontaneous decay into cavity mode i.

Analytical solution—With the model above, we are ready to solve the rate equations and obtain two thresholds. For an analytical treatment, we restrict ourselves to the smallest number of modes needed to observe the second threshold, $\mathscr{M} = 2$. To find the pump threshold frequency at which the condensation forms, we first algebraically solve the steady-state condition $\dot{n}_2 = 0$ for $n_2 = n_2(n_1)$. The explicit form is written in Ref. [25]. Next, we solve $(\partial^3 n_2/\partial\Gamma_{\uparrow}^3)_{n_1} = 0$ to

obtain $\Gamma_{\uparrow} = \Gamma_{\uparrow}(n_1)$. This approach is inspired by the fact that the second derivative of the single mode solution $\mathrm{d}^2 n_1/\mathrm{d}\Gamma_{\uparrow}^2$ in the limit of small cavity decay [23] gives a Dirac delta function at the first threshold position $\Gamma_{\uparrow} = \Gamma_{\uparrow}^{th1}$, see more details in Ref. [25]. The explicit solution of $\Gamma_{\uparrow}(n_1)$ [25] marks the special points where n_2 changes its behavior and indicates the condensation point. To proceed further, we solve the single-mode equation $\dot{n}_1 = 0$ [23] and find $n_1(\Gamma_{\uparrow})$ [25]. We substitute the solution into the threshold condition for $\Gamma_{\uparrow} = \Gamma_{\uparrow}(n_1)$ and solve for $\Gamma_{\uparrow}$, leading to two solutions as threshold conditions. Expanding them to the first order in κ/M which is a small parameter compared to α_i, ϵ_i, and assuming $\epsilon_2 \approx \epsilon_1$, and $\alpha_2 \approx \alpha_1$ for small mode spacings, they read

$$\Gamma_{\uparrow}^{th1} = \frac{(\Gamma_{\downarrow} + \epsilon_1)\alpha_1}{\epsilon_1},$$
$$\Gamma_{\uparrow}^{th2} = \frac{\Gamma_{\downarrow}\alpha_1}{\epsilon_1} + \frac{\alpha_1(\epsilon_1 + \alpha_1)\kappa}{M|\epsilon_2\alpha_1 - \epsilon_1\alpha_2|}. \quad (2)$$

For small mode spacings $\Delta k^{\parallel}$, the populations n_i in all modes below $\Gamma_{\uparrow}^{th1}$ are comparable up to the degeneracy factor g_i. Above $\Gamma_{\uparrow}^{th1}$, the populations equally rise together and occupy the system macroscopically. Above $\Gamma_{\uparrow}^{th2}$, the populations in excited modes saturate, and n_1 assumes a macroscopic fraction of the total photon number.

The first threshold $\Gamma_{\uparrow}^{th1}$ is similar as in Ref. [23], except for the extra ϵ_1 term in the brackets. The second threshold $\Gamma_{\uparrow}^{th2}$ is separated from $\Gamma_{\uparrow}^{th1}$ by an amount linearly dependent on κ, inversely proportional to M and to the difference between absorption and emission rates. This implies that at infinitesimal mode spacing, the denominator tends to zero, and consequently, $\Gamma_{\uparrow}^{th2}$ approaches infinity. We see that $\Gamma_{\uparrow}^{th2}$ is determined by the competition between mode width κ and $|\epsilon_2\alpha_1 - \epsilon_1\alpha_2|$ which is determined by the mode separation $\Delta k^{\parallel}$. In Supplemental Material [25] we show how $\Gamma_{\uparrow}^{th2}$ is directly related to $\Delta k^{\parallel}$. It is noteworthy to mention that each threshold is mainly governed by one of two characteristic loss channels in our system: The first threshold is determined by the spontaneous emission of molecules $\Gamma_{\downarrow}$, while the second threshold is induced by the cavity decay κ.

Numerical solutions—We now turn to numerical simulations of the photon population for more modes and demonstrate the steady state behavior for different mode spacings together with the thresholds from Eq. (2). The numerical parameters used in this Letter are shown in Supplemental Material [25]. The steady-state photon populations as a function of pumping rate $\Gamma_{\uparrow}$ are shown in Figs. 1(a) to 1(c), up to the degeneracy factor g_i. In Fig. 1(a), the mode spacing is sufficiently large so that the first and second thresholds coincide. We observe a sharp increase in all populations at the first threshold, and for
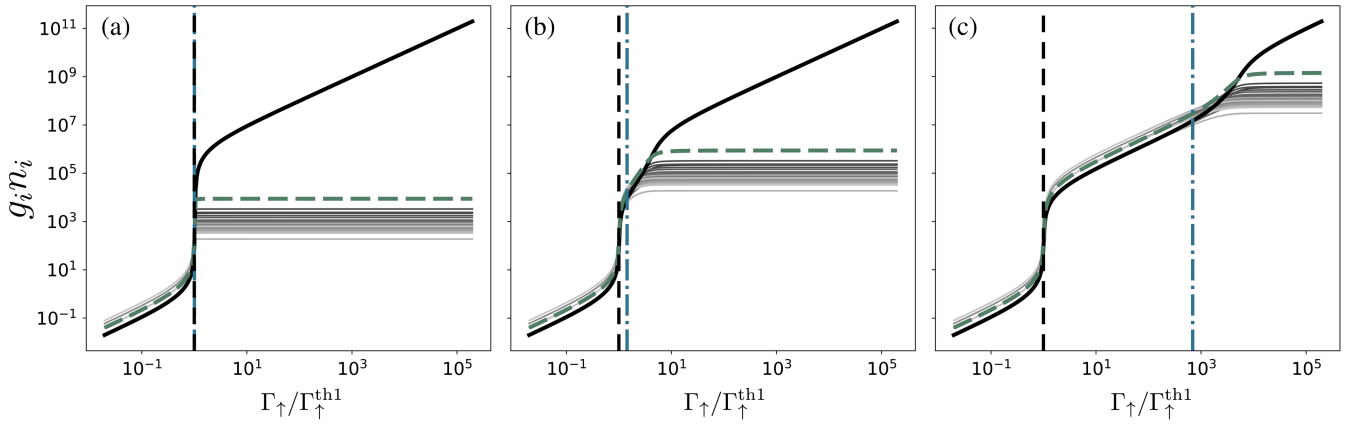
FIG. 1. Mode populations $g_i n_i$ in a steady state as a function of normalized pump rate where graphs from (a)–(c) are in order of decreasing mode spacing, $\Delta k^{\parallel} = 2 \times 10^4, 2 \times 10^3, 50$ m^{-1}, respectively. The thick black and the green dashed curves are the ground and first excited states, respectively. The gray lines are all the other excited modes. The corresponding vertical dashed and dot-dashed lines show the value of the thresholds $\Gamma_{\uparrow}^{\text{th1}}$ and $\Gamma_{\uparrow}^{\text{th2}}$. Here, $\Gamma_{\uparrow}^{\text{th1}} \approx 5.1 \times 10^6$ Hz. The simulations include 30 modes.

increasing pumping rate the ground mode separates from all excited modes which saturate at constant values. In Fig. 1(b), we observe a separation of $\Gamma_{\uparrow}^{\text{th2}}$ from $\Gamma_{\uparrow}^{\text{th1}}$. Furthermore, the behavior of populations is qualitatively different compared to Fig. 1(a): The excited mode populations saturate for higher pump values, while in ground mode populations we observe a kink above the second threshold. We refer to this region between both thresholds as the precondensate region where the condensate is not fully formed as the ground mode occupation grows in tandem with the occupation of the neighboring modes. Alternatively, this region may be referred to as the supercooling region in analogy with the supercooling of water between the freezing and the crystal homogeneous nucleation points. Finally, in Fig. 1(c), the second threshold is completely separated from the first threshold. All populations increase simultaneously, and above $\Gamma_{\uparrow}^{\text{th2}}$ only the ground mode continues to grow. We see that $\Gamma_{\uparrow}^{\text{th2}}$ marks the separation of the ground mode from the other modes for all three cases, while $\Gamma_{\uparrow}^{\text{th1}}$ remains fixed. As we decrease $\Delta k^{\parallel}$, a larger pump rate is required for full condensation. Ultimately, in the limit of the free 2D photon gas, the ground mode will only separate at an infinite pump rate.

The method of finding the zero crossing of $\partial^3 n_2 / \partial \Gamma_{\uparrow}^3$ allows us to numerically obtain the second threshold values for larger mode numbers, whose analytical expression is not attainable. We call it the exact second threshold $\tilde{\Gamma}_{\uparrow}^{\text{th2}} = \Gamma_{\uparrow}|_{d^3 n_2 / d\Gamma_{\uparrow}^3 = 0}$ which marks an exact position of the condensation for any mode number. For $\mathscr{M} = 2$, we have $\Gamma_{\uparrow}^{\text{th2}} \approx \tilde{\Gamma}_{\uparrow}^{\text{th2}}$ and in Supplemental Material [25] we show a deviation of $\Gamma_{\uparrow}^{\text{th2}}$ from $\tilde{\Gamma}_{\uparrow}^{\text{th2}}$. Figure 2(a) shows $\tilde{\Gamma}_{\uparrow}^{\text{th2}}$ as a function of the mode number with a monotonic increase. Figure 2(a) shows that $\Gamma_{\uparrow}^{\text{th2}}$ marks the condensation point too early for larger mode numbers. Despite that, $\Gamma_{\uparrow}^{\text{th2}}$ can still

qualitatively describe the threshold point for decreasing $\Delta k^{\parallel}$, as shown in Fig. 2(b). We see how $\Gamma_{\uparrow}^{\text{th2}}$ consistently marks the kink of the ground mode towards its linear condensed asymptote even for 30 modes. For comparison, we show the position of $\tilde{\Gamma}_{\uparrow}^{\text{th2}}$ obtained for 30 modes. We see that $\tilde{\Gamma}_{\uparrow}^{\text{th2}}$ marks the condensation point more precisely, as expected.

Thermodynamic solution—To analyze $\Gamma_{\uparrow}^{\text{th2}}$ further, we relate it to the critical particle number obtained by counting the photons in the Bose-Einstein distribution. We can analytically evaluate the critical photon number assuming a paraxial approximation, $k_x, k_y \ll k_z$. Following along the lines of [28,29], we obtain the critical photon number N_c in a 2D system for small mode spacing $\Delta k^{\parallel}$:

$$N_c^{(\infty)} = \sum_{j_x, j_y=1}^{\infty}{}' [e^{\beta \hbar [\omega(j_x, j_y) - \omega(1,1)]} - 1]^{-1} \approx -\frac{\pi}{2} \frac{1}{s} \ln s, \quad (3)$$
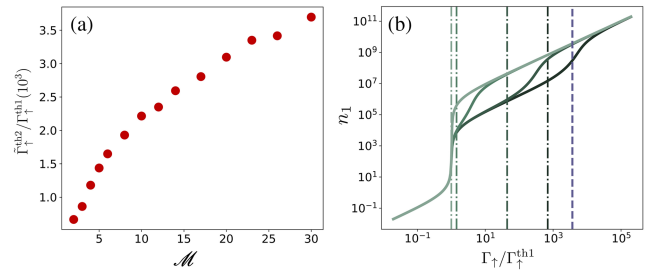

FIG. 2. (a) Value of the exact threshold $\tilde{\Gamma}_{\uparrow}^{\text{th2}}$ as a function of the mode number $\mathscr{M}$. Here, $\Delta k^{\parallel} = 50$ m^{-1}. (b) Ground mode populations simulated for 30 modes. Each curve depicts four different mode spacings in a decreasing value from left to right ($\Delta k^{\parallel} = 2 \times 10^4, 2 \times 10^3, 2 \times 10^2, 50$ m^{-1}) (lighter to darker shades of green). Vertical dot-dashed lines indicate the second threshold $\Gamma_{\uparrow}^{\text{th2}}$ for each respective mode spacing. The vertical purple dashed line depicts $\tilde{\Gamma}_{\uparrow}^{\text{th2}}$ for $\Delta k^{\parallel} = 50$ m^{-1}.
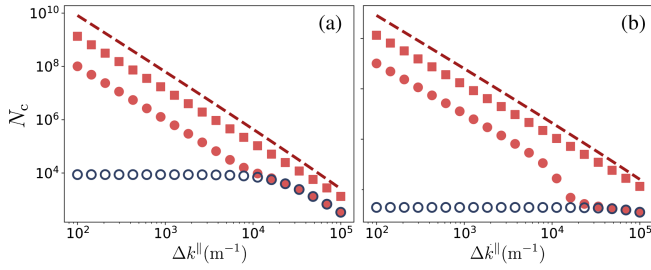
FIG. 3. Critical number of particles as a function of the mode spacing $\Delta k^{\parallel}$ with (a) $\kappa = 0.05$ and (b) $\kappa = 5$ GHz. Red-filled and blue hollow dots depict critical numbers for $\mathscr{M} = 2$ obtained from values of $\Gamma_{\uparrow}^{\mathrm{th2}}$ and $\Gamma_{\uparrow}^{\mathrm{th1}}$ in Eq. (2), respectively. Red squares illustrate N_c obtained from $\tilde{\Gamma}_{\uparrow}^{\mathrm{th2}}$ for $\mathscr{M} = 30$. The dashed line depicts the thermodynamic solution from Eq. (3).

where $s = \beta \hbar c (\Delta k^{\parallel})^2 / k_z \sqrt{\epsilon}$ and in the primed sum we have excluded the pair $(j_x, j_y) = (1, 1)$. To relate the two thresholds from Eq. (2) with the photon number, we substitute the values into Eqs. (1) and solve for the total photon number in all the excited states $N_{\mathrm{ex}}(\Gamma_{\uparrow})$, obtaining two critical photon numbers, $N_{\mathrm{ex}}(\Gamma_{\uparrow}^{\mathrm{th1}}) \equiv N_c^{(1)}$ and $N_{\mathrm{ex}}(\Gamma_{\uparrow}^{\mathrm{th2}}) \equiv N_c^{(2)}$. For $\mathscr{M} = 2$, we have $N_{\mathrm{ex}} \equiv g_2 n_2$.

Figure 3 compares the critical photon numbers $N_c^{(1)}$, $N_c^{(2)}$, and $N_c^{(\infty)}$ for decreasing mode spacing. At small $\Delta k^{\parallel}$ the behavior of $N_c^{(2)}$ is qualitatively similar to $N_c^{(\infty)}$, i.e., both numbers tend to infinity as $\Delta k^{\parallel} \to 0$. An offset is present between $N_c^{(\infty)}$ and $N_c^{(2)}$ which is expected since the critical photon number from Eq. (2) has been obtained by assuming only two modes in the cavity, while Eq. (3) assumes infinitely many modes. Crucially, we see that $N_c^{(1)}$ fails to predict the critical number for small mode spacings as it saturates, similarly as in Fig. 1. For large mode spacings, $N_c^{(1)}$ and $N_c^{(2)}$ coincide. Comparing Figs. 3(a) and 3(b) we see that for smaller cavity decay rates, $N_c^{(1)}$ separates from $N_c^{(2)}$ at smaller $\Delta k^{\parallel}$ value than for larger κ, consistent with Eq. (2). Moreover, the qualitative behavior of $N_c^{(2)}$ around the separation point indicates higher nonlinearity for larger values of κ.

For comparison, in Fig. 3 we also show the critical photon number obtained with $\tilde{\Gamma}_{\uparrow}^{\mathrm{th2}}$ for 30 modes (also see Fig. 2). Naturally, we observe that for higher mode numbers the critical photon number approaches $N_c^{(\infty)}$.

Supercooling region—As seen in Figs. 1 and 2(b), for small $\Delta k^{\parallel}$, the second threshold diverges and the supercooling region extends to larger pumping strengths. Therefore, it is insightful to investigate further the behavior of the difference between photons in the ground and excited modes. Since populations in the neighboring modes in the supercooling region are similar, as seen in Fig. 1(c), it is possible to utilize the perturbation method for a generic

number of modes. We expand the occupation in mode i perturbatively, $n_i = n_1 + q_i \Delta n$ for $i \geq 2$, where Δn is a small difference in photon number and q_i are mode-dependent coefficients. We choose $q_2 = 1$ without loss of generality. In a similar manner, we express the absorption and emission rates as $\alpha_i = \alpha_1 + \mu_i \Delta \Gamma$ and $\varepsilon_i = \varepsilon_1 + \eta_i \Delta \Gamma$, where $\Delta \Gamma$ is a small deviation proportional to the mode spacing. Again, μ_i and η_i are the mode-dependent coefficients where we choose $\mu_2 \equiv 1$ and $\eta_2 \equiv \eta$. With these assumptions and only retaining the lowest orders of $\Delta \Gamma$ and Δn, we can solve Eqs. (1) analytically for $\mathscr{M} = 2$ or higher. For a nondegenerate ground mode $g_1 = 1$, in the limit of small cavity decay κ we obtain the solution for Δn:

$$\Delta n = \begin{cases} n_1^2 \dfrac{(\varepsilon_1 - \alpha_1 \eta) \Delta \Gamma}{\alpha_1 \varepsilon_1}, & \Gamma_{\uparrow} \geq \Gamma_{\uparrow}^{\mathrm{th1}}, \\ 0, & \text{otherwise.} \end{cases} \quad (4)$$

Here, n_1 is the photon occupation of the ground mode:

$$n_1 = \begin{cases} \dfrac{M(\varepsilon_1 \Gamma_{\uparrow} - \alpha_1 \Gamma_{\downarrow})}{(1 + \sum_{i=2}^{\mathscr{M}} g_i)(\alpha_1 + \varepsilon_1) \kappa}, & \Gamma_{\uparrow} \geq \Gamma_{\uparrow}^{\mathrm{th1}}, \\ 0, & \text{otherwise.} \end{cases} \quad (5)$$

The solution (4) indicates a sharp transition above $\Gamma_{\uparrow}^{\mathrm{th1}}$ with a linear growth for increasing $\Delta \Gamma$, similarly as for the single mode discussed in Ref. [23]. The transition becomes less pronounced for a higher number of modes or larger degeneracies since Δn is inversely proportional to $\mathscr{M}$ and g_i. Figure 4 shows the dependence of $|\Delta n|$ for different values of $\Delta \Gamma$. Evidently, we see the breakdown of linearity
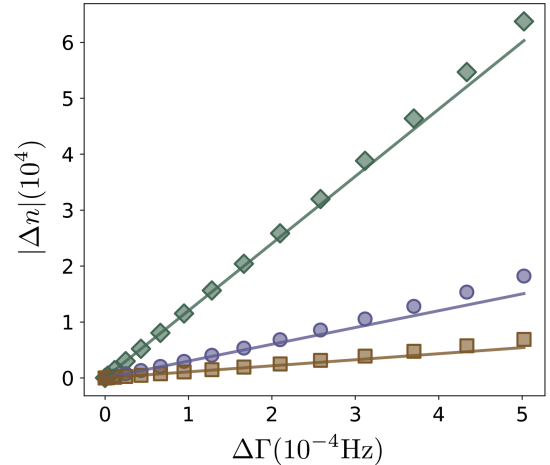

FIG. 4. Absolute value of the difference between ground and first excited mode $|\Delta n|$ as a function of $\Delta \Gamma$ for different mode numbers $\mathscr{M} = 2$ (green rhomboids), 4 (purple circles), 6 (red squares). Solid lines are the analytical expression from Eq. (4). Here, the value of the pump rate is $\Gamma_{\uparrow} = 2 \Gamma_{\uparrow}^{\mathrm{th1}}$.

of $|\Delta n|$ for larger values of $\Delta\Gamma$. If higher orders of κ were retained, the correspondence between numerics and analytics would match at higher values of $\Delta\Gamma$. Note that our solution is only valid in the region $\Gamma_\uparrow^{th1} \leq \Gamma_\uparrow < \Gamma_\uparrow^{th2}$.

The solution (5) is similar to that in Ref. [23], except for the correction factor in the denominator which depends on degeneracies and the number of modes. For an increasingly large system, the condensation transition becomes less distinct, similarly as for Δn. As a result, in the limit $\mathcal{M} \to \infty$ for a free photon gas, our findings indicate $\Delta n \to 0$ and $n_1 \to 0$ for a fixed $\Gamma_\uparrow$. Since Δn vanishes, the populations in any mode i coincide with the ground mode, $n_i \to n_1$, up to a degeneracy factor.

Conclusions—In this Letter, we have demonstrated the emergence of a second condensation threshold in the regime of small mode spacing of a two-dimensional photon gas in a planar cavity, which is inversely proportional to the mode spacing. The first and second thresholds are governed by system losses. At the second threshold, the ground mode becomes dominant in a different fashion compared to the case of larger mode spacing. From analytical and numerical solutions, we see how the phase transition disappears in the limit of a free 2D photon gas. We have found this to be caused by an infinite growth of the second threshold value.

The intermediate region between the two thresholds, referred to as the supercooling region, is marked by incomplete condensation. Here, the separation in occupation between ground and first excited modes is linear in the mode spacing, hindering the system from reaching a fully condensed regime. Our analysis shows that potential uses of the photon BEC, such as the quantum sensor [23], will have to operate at a sufficiently large pumping rate to overcome the second threshold. Furthermore, our results are relevant for studies of open systems with a driven dissipative nature, as well as systems at the crossover towards continuum spectra.

[1] C. J. Pethick and H. Smith, *Bose-Einstein Condensation in Dilute Gases* (Cambridge University Press, Cambridge, England, 2008).

[2] K. B. Davis, M.-O. Mewes, M. R. Andrews, N. J. van Druten, D. S. Durfee, D. M. Kurn, and W. Ketterle, Bose-Einstein condensation in a gas of sodium atoms, Phys. Rev. Lett. **75**, 3969 (1995).

[3] J. Klaers, J. Schmitt, F. Vewinger, and M. Weitz, Bose-Einstein condensation of photons in an optical microcavity, Nature (London) **468**, 545 (2010).

[4] J. Schmitt, Dynamics and correlations of a Bose-Einstein condensate of photons, J. Phys. B **51**, 173001 (2018).

[5] R. May, Superconductivity of a charged ideal 2-dimensional Bose gas, Phys. Rev. **115**, 254 (1959).

[6] P. C. Hohenberg, Existence of long-range order in one and two dimensions, Phys. Rev. **158**, 383 (1967).

[7] V. Bagnato and D. Kleppner, Bose-Einstein condensation in low-dimensional traps, Phys. Rev. A **44**, 7439 (1991).

[8] K. Kirsten and D. J. Toms, Simple criterion for the occurrence of Bose-Einstein condensation, Phys. Lett. B **368**, 119 (1996).

[9] J. Schmitt, T. Damm, D. Dung, F. Vewinger, J. Klaers, and M. Weitz, Observation of grand-canonical number statistics in a photon Bose-Einstein condensate, Phys. Rev. Lett. **112**, 030401 (2014).

[10] J. Marelic and R. A. Nyman, Experimental evidence for inhomogeneous pumping and energy-dependent effects in photon Bose-Einstein condensation, Phys. Rev. A **91**, 033813 (2015).

[11] J. Schmitt, T. Damm, D. Dung, F. Vewinger, J. Klaers, and M. Weitz, Thermalization kinetics of light: From laser dynamics to equilibrium condensation of photons, Phys. Rev. A **92**, 011602(R) (2015).

[12] J. Schmitt, T. Damm, D. Dung, C. Wahl, F. Vewinger, J. Klaers, and M. Weitz, Spontaneous symmetry breaking and phase coherence of a photon Bose-Einstein condensate coupled to a reservoir, Phys. Rev. Lett. **116**, 033604 (2016).

[13] T. Damm, D. Dung, F. Vewinger, M. Weitz, and J. Schmitt, First-order spatial coherence measurements in a thermalized two-dimensional photonic quantum gas, Nat. Commun. **8**, 158 (2017).

[14] M. Radonjić, W. Kopylov, A. Balaž, and A. Pelster, Interplay of coherent and dissipative dynamics in condensates of light, New J. Phys. **20**, 055014 (2018).

[15] F. E. Ozturk, T. Lappe, G. Hellmann, J. Schmitt, J. Klaers, F. Vewinger, J. Kroha, and M. Weitz, Fluctuation dynamics of an open photon Bose-Einstein condensate, Phys. Rev. A **100**, 043803 (2019).

[16] F. E. Öztürk, T. Lappe, G. Hellmann, J. Schmitt, J. Klaers, F. Vewinger, J. Kroha, and M. Weitz, Observation of a non-Hermitian phase transition in an optical quantum gas, Science **372**, 88 (2021).

[17] F. E. Öztürk, F. Vewinger, M. Weitz, and J. Schmitt, Fluctuation-dissipation relation for a Bose-Einstein condensate of photons, Phys. Rev. Lett. **130**, 033602 (2023).

[18] E. Busley, L. E. Miranda, A. Redmann, C. Kurtscheid, K. K. Umesh, F. Vewinger, M. Weitz, and J. Schmitt, Compressibility and the equation of state of an optical quantum gas in a box, Science **375**, 1403 (2022).

[19] H. Li, Q. Guo, J. Jiang, and D. C. Johnston, Thermodynamics of the noninteracting Bose gas in a two-dimensional box, Phys. Rev. E **92**, 062109 (2015).

[20] R. A. Nyman and B. T. Walker, Bose-Einstein condensation of photons from the thermodynamic limit to small photon numbers, J. Mod. Opt. **65**, 754 (2018).

[21] J. D. Rodrigues, H. S. Dhar, B. T. Walker, J. M. Smith, R. F. Oulton, F. Mintert, and R. A. Nyman, Learning the fuzzy

phases of small photonic condensates, Phys. Rev. Lett. **126**, 150602 (2021).

[22] M. Beau and V. A. Zagrebnov, Quasi-one-and quasi-two-dimensional perfect Bose gas: The second critical density and generalised condensation, Condens. Matter Phys. **12**, 23003 (2010).

[23] R. Bennett, D. Steinbrecht, Y. Gorbachev, and S. Y. Buhmann, Symmetry breaking in a condensate of light and its use as a quantum sensor, Phys. Rev. Appl. **13**, 044031 (2020).

[24] Zenodo: 10.5281/zenodo.10852936.

[25] See Supplemental Material at http://link.aps.org/supplemental/10.1103/PhysRevLett.133.223601, which includes Refs. [23,24], for more details.

[26] P. Kirton and J. Keeling, Nonequilibrium model of photon condensation, Phys. Rev. Lett. **111**, 100404 (2013).

[27] S. Y. Buhmann and A. Erglis, Nested-open-quantum-systems approach to photonic Bose-Einstein condensation, Phys. Rev. A **106**, 063722 (2022).

[28] A. Chaba and R. Pathria, Bose-Einstein condensation in a two-dimensional system at constant pressure, Phys. Rev. B **12**, 3697 (1975).

[29] H. Kleinert, *Path Integrals in Quantum Mechanics, Statistics, Polymer Physics, and Financial Markets* (World Scientific, Singapore, 2009).